INTERNATIONAL JOURNAL FOR NUMERICAL METHODS IN FLUIDS
Int. J. Numer. Meth. Fluids 2006; **51**:1079–1095
Published online in Wiley InterScience (www.interscience.wiley.com). DOI: 10.1002/fld.1289

Higher-resolution hyperbolic-coupled-elliptic flux-continuous CVD schemes on structured and unstructured grids in 3-D

Michael G. Edwards*, †

Civil and Computational Engineering Centre, School of Engineering, University of Wales Swansea, Singleton Park, Swansea SA2 8PP, U.K.

SUMMARY

Novel three-dimensional unstructured grid higher order convection schemes are presented. The schemes are coupled with locally conservative flux continuous control-volume distributed (CVD) finite-volume schemes for the porous medium general tensor pressure equation on structured and unstructured grids in 3-D.

The schemes are developed for multi-phase flow in porous media. Benefits of the schemes in terms of improved front resolution and medium discontinuity resolution are demonstrated. Comparisons with current methods including the control-volume finite element method highlight the advantages of the new formulation for three-dimensional reservoir simulation. Copyright © 2006 John Wiley & Sons, Ltd.

Received 2 June 2005; Revised 4 April 2006; Accepted 27 April 2006

KEY WORDS: higher-order; flux-continuous; full-tensor; finite-volume; unstructured

1. INTRODUCTION

The focus of this paper is on the development of three-dimensional higher order convection schemes coupled with optimal discrete continuous Darcy fluxes for approximation of the multi-phase flow equations that arise in reservoir simulation. The system of equations considered here is hyperbolic fluid transport coupled with an elliptic system for pressure and Darcy velocity [1], see also Reference [2].

A novel higher order scheme with maximum principle for unstructured grids in three dimensions is presented. The higher order convection schemes presented here extend the two-dimensional hyperbolic schemes presented in Reference [3] to 3-D. Higher order convection schemes for

*Correspondence to: Michael G. Edwards, Civil and Computational Engineering Centre, School of Engineering, University of Wales Swansea, Singleton Park, Swansea SA2 8PP, U.K.
†E-mail: m.g.edwards@swansea.ac.uk

Contract/grant sponsor: EPSRC; contract/grant number: GR/S70968/01

reservoir simulation have been developed over a number of years, e.g. References [3–11]. These schemes achieve higher order accuracy and are constructed such that the solution remains free of spurious oscillations. These methods yield benefits in terms of improved front resolution and have been successfully demonstrated for a variety of multi-phase flow problems in subsurface reservoir simulation.

The continuous Darcy flux schemes presented here are a three-dimensional generalization of the two-dimensional elliptic schemes presented in Reference [3]. Previous work in the area of locally conservative flux-continuous full-tensor finite-volume schemes includes References [12–26]. The schemes presented here are control-volume distributed (CVD) where flow variables and rock properties are associated with the control-volumes of the grid and provide a consistent discretization of the porous medium pressure equation applicable to general geometry and permeability tensors on structured and unstructured grids e.g. Reference [12]. Mixed finite element methods (MFEM) e.g. References [7, 27–31] preserve flux continuity for full tensor flows, however mixed methods solve for velocity components and pressure in a globally coupled system. For a three-dimensional structured grid MFEM involve solving for four times as many degrees of freedom as (the more efficient) CVD methods. The CVD schemes presented here maintain flux continuity with one discrete pressure value per control-volume.

Coupling of the novel higher order phase component approximations with the general tensor flux-continuous formalism is a new development for general grids in three dimensions. Here *general* is used in the sense of allowing the grid to be composed of any element type, arbitrary distortions of such grids and their effects remain to be investigated. The new formulation yields an improved scheme for reservoir simulation applicable to multi-phase flow while using an optimal number of degrees of freedom within the discretization.

Flow equations are presented in Section 2. A brief summary of the three-dimensional flux continuous formulation is presented in Section 3. Extension of the higher order schemes to general unstructured grids is presented in Section 4. Two-phase flow results are presented in Section 5 that demonstrate the advantages of the new higher order flux-continuous formulation in terms of grid orientation and front resolution. Comparisons with the standard control-volume finite element CVFE scheme [32], (exactly the same number of degrees of freedom), demonstrate advantages of the new formulation with respect to medium discontinuity resolution for reservoir simulation. Conclusions are presented in Section 6.

2. FLOW EQUATIONS

The flow equations are briefly described here, the reader is referred to Reference [1] for a comprehensive account. The schemes presented here are illustrated with respect to two phase incompressible flow models, where without loss of generality unit porosity is assumed and capillary pressure and dispersion are neglected. The integral form of the flow equations is given over a control-volume Ω_{cv} with surface $\partial\Omega_{\mathrm{cv}}$, the continuity equations for phases $p = 1, N_p$ are written as

$$\int_{\Omega_{\mathrm{cv}}} \left(\frac{\partial S_p}{\partial t} + \nabla \bullet \mathbf{V}_p \right) \mathrm{d}\tau = m_p \tag{1}$$

where S_p, $\mathbf{V}_p$ and m_p are the pth phase saturation, Darcy velocity (defined below) and specified phase flow rate, respectively, and phase saturations sum to unity.

DOI: 10.1002/fld

The momentum equations are defined through Darcys law where the pth phase velocity is defined by

$$\mathbf{V}_p = \mathrm{f}_p(\mathbf{V}_T - \triangle\rho(\mathbf{S})g\mathbf{K}\nabla h) \tag{2}$$

here f_p is the fractional flow of phase p, and $\mathbf{V}_T$ is the total Darcy velocity defined via

$$\mathbf{V}_T = -\Lambda\mathbf{K}(\nabla\phi + \bar{\rho}g\nabla h) \tag{3}$$

where Λ is the total mobility [1], $\mathbf{K}$ is a diagonal or full elliptic Cartesian permeability tensor, ϕ is the pressure and $\nabla = \partial_{x_i}$.

Also, $\bar{\rho} = \sum_{p=1}^{N_p} \rho_p\lambda_p/\Lambda$ is the mean density and λ_p, ρ_p are the pth phase mobility and density, respectively, $\triangle\rho(\mathbf{S}) = (\rho_p - \bar{\rho})$, h is the height, g the acceleration due to gravity.

The closed surface integral of phase velocity can now be expressed as the sum of outward normal phase fluxes F_{p_i} over each of the surface increments of the control-volume Ω_{cv}, viz

$$\oint_{\partial\Omega_{\mathrm{cv}}} \mathbf{V}_p \bullet \hat{\mathbf{n}}\,\mathrm{d}s = \sum_{i=1}^{N_S} \mathrm{F}_{p_i} \tag{4}$$

where N_S is the number of surface increments that enclose the volume Ω_{cv}. The outward normal phase flux in the ith normal direction is written in terms of the general tensor $\mathbf{T}$ as

$$\mathrm{F}_{p_i} = -\int_{\partial\Omega_{\mathrm{cv}}} \mathrm{f}_p\Lambda\left(\sum_{j=1}^{3} T_{ij}\phi_{\xi_j} + \rho_p g\sum_{j=1}^{3} T_{ij}h_{\xi_j}\right)\mathrm{d}\Gamma_i \tag{5}$$

where ξ_i are local curvilinear parametric coordinates, Γ_i is the parametric coordinate surface increment and ϕ_{ξ_j} is the derivative of ϕ with respect to ξ_j and

$$\mathbf{T} = J\mathbf{J}^{-1}\mathbf{K}\mathbf{J}^{-\mathrm{T}} \tag{6}$$

is the general tensor defined via the Piola transformation which is function of the Cartesian permeability tensor and geometry, where $J_{ij} = \partial x_i/\partial\xi_j$ is the Jacobian of the local curvilinear coordinate transformation. General full tensors can arise (with non-zero cross terms $T_{ij} \neq 0$ for $i \neq j$) as a result of the grid type, local orientation of the grid and permeability field and from upscaling. For incompressible flow Equation (1) is summed over the N_p phases and since saturations sum to unity, using Equations (4) and (5) the pressure equation

$$\sum_{i=1}^{N_S} \mathrm{F}_{T_i} = M \tag{7}$$

is obtained. In order to simplify notation gravity will now be omitted from the formalism, however once the discrete flux is defined gravity can be included by following the above definitions. Now using

$$\mathrm{F}_{p_i} = -\int_{\partial\Omega_{\mathrm{cv}}} \mathrm{f}_p\Lambda\sum_{j=1}^{3} T_{ij}\phi_{\xi_j}\,\mathrm{d}\Gamma_i \tag{8}$$

DOI: 10.1002/fld

the total flux is given by

$$\mathrm{F}_{T_i} = -\int_{\partial\Omega_{\mathrm{cv}}} \Lambda \sum_{j=1}^{3} T_{ij}\,\phi_{\xi_j}\,\mathrm{d}\Gamma_i \tag{9}$$

and involves a product of total mobility and single phase flux. Note that the single phase flux is obtained by setting $\Lambda = 1$ in Equation (9). Zero normal flux (Neumann) applies on solid walls, here M is the total inflow/outflow flux which is zero away from wells. Initial data in terms of saturation and pressure fields are also prescribed. Further details can be found in Reference [1].

3. FLUX-CONTINUOUS CONTROL-VOLUME DISTRIBUTED (CVD) APPROXIMATIONS IN 3-D

The initial or primal grid is comprised of cells, with corners defined by the grid vertices. The distinction between cell centred and cell vertex schemes is discussed in Reference [3]. The schemes presented here are vertex centred, where for a given control-volume surrounding a grid vertex, flow variables are assigned to grid vertices *and* rock properties are piecewise constant with respect to the control-volumes and are CVD. The physical constraints that must be enforced are continuity of pressure and continuity of normal flux across interfaces (control-volume faces) that separate changes in permeability tensor.

3.1. Continuous flux approximation in three dimensions

We now consider approximation of the incompressible single phase flow pressure equation and present a summary of the flux-continuous formulation in three dimensions. Previous work on flux-continuous schemes in 3-D is presented in References [15, 20, 23, 25]. The primal grid considered here can be a hybrid composed of combinations of tetrahedra, prisms, pyramids and hexahedra elements in 3-D. In principle the only restriction on grid structure is that tetrahedra can only be joined to hexahedra through a pyramid interface. A polyhedral control-volume is built around each grid vertex, generating a primal-dual grid. Starting in a primal grid cell, the cell centre is joined to cell face mid-points, cell face mid-points are joined to cell edge mid-points. As a result the primal grid cells are decomposed into sub-hexahedra or subcells, four for a tetrahedra, five for a pyramid, six for a prism and eight for a hexahedra. In each case the number of subcells corresponds to the number of vertices defining the primal cell, and each subcell belongs to the control-volume of the unique vertex to which it is attached. Cell vertex control-volumes are defined by a local assembly or recomposition at each primal grid vertex of all subcells that are attached to the vertex. The resulting set of polyhedral control-volumes defines a dual grid relative to the primal grid which we call the primal-dual. Rock permeability and porosity are assumed to be piece-wise constant over each polyhedral control-volume and flow variables belong to the control-volumes and are vertex centred. Figures 1 and 2. Therefore, discontinuities in rock properties occur over the control-volume faces.

As with all finite volume schemes we begin with application of the Gauss divergence theorem to the integral of divergence, cf. Equation (1) over a given control-volume. A unique discrete flux is then constructed for each control-volume face and the closed integral of flux is approximated by the sum of discrete outward normal fluxes. For a given face between two neighbouring control-volumes, the unique flux is subtracted from the left-hand control-volume and added to the right-hand

DOI: 10.1002/fld

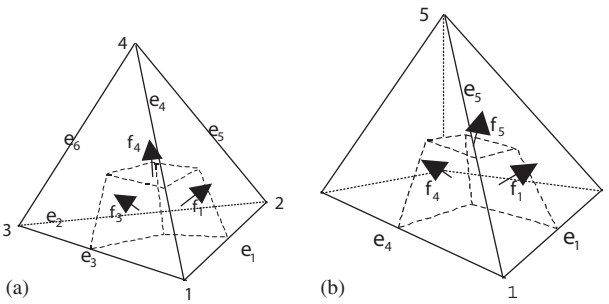

Figure 1. Subcell (dashed line) of the control-volume surrounding primal cell vertex local number 1, for: (a) tetrahedra; and (b) pyramid.

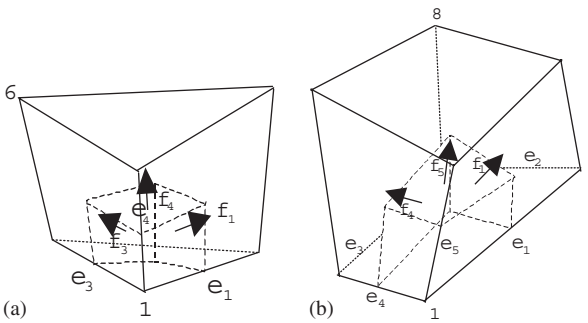

Figure 2. Subcell (dashed line) of the control-volume surrounding primal cell vertex local number 1, for: (a) prism; and (b) hexahedra.

control-volume leading to a locally conservative scheme with respect to the faces of the polyhedral control volumes that contain the discrete permeability tensors with flow variables defined at their vertices.

Within the flux build process, fluxes are approximated on control-volume subcell faces inside each primal grid cell, in analogous steps to 2-D [3]. Flux continuity conditions are discussed in the next subsection. Each subcell flux is associated with a unique cell edge, the number of (primal-cell) fluxes constructed inside each primal cell is equal to the number of edges, 12 for a hexahedra, 9 for a prism, 8 for a pyramid and 6 for a tetrahedra.

The subcell fluxes are accumulated with respect to their primal cell edges within an assembly process. The edge index $e(i, j)$ refers to the jth primal edge attached to vertex i. The net edge-based single phase flux $F_{e(i,j)}(\phi)$ associated with edge $e(i, j)$ is comprised of the sum of adjacent subcell fluxes that belong to the primal grid cells with common edge $e(i, j)$, with

$$F_{e(i,j)}(\phi) = \sum_{\sigma=1}^{N_{\mathrm{SCE}}} F_{\sigma}(\phi) \tag{10}$$

where N_{SCE} is the number of subcells attached to the edge $e(i, j)$. After assembly of net edge-based fluxes, the discrete scheme for each vertex i is completed with the closed integral of net

DOI: 10.1002/fld

Gaussian flux approximated by the sum of net edge-based fluxes connected to the ith vertex. For single phase flow on unstructured grids the assembled finite volume scheme at vertex i can be written concisely as

$$\sum_{j=1}^{N_{\mathrm{edV}}} F_{e(i,j)}(\phi) = M_i \tag{11}$$

where summation is over all N_{edV} edges passing through the ith grid vertex, (M_i denotes a specified flow rate at vertex i, or is zero otherwise).

3.2. *Control-volume flux and continuity*

Here a summary of the continuous algebraic flux approximation is given. A consistent normal flux approximation is constructed such that pressure and normal flux are continuous across control-volume faces inside a primal grid cell. In order to achieve this (as in 2-D [3]) local interface pressures are introduced, one per control-volume sub-face, establishing point-wise continuity in pressure. Subcell tetrahedral basis functions are then formed by joining the cell vertices (with locally numbered vertex pressures $\mathbf{\Phi}_v$) to the positions of the adjacent interface pressures $\mathbf{\Phi}_f$ and three normal fluxes are defined with respect to each subcell (with exception of pyramid summit), on the three faces of each subcell that are inside the primal grid cell. Flux continuity is then imposed by equating fluxes on the left- and right-hand sides (L, R) of each of the interfaces in each primal cell resulting in

$$F_i = -\beta(T_{i1}\phi_\xi + T_{i2}\phi_\eta + T_{i3}\phi_\zeta)|_\sigma^{\mathrm{L}} = -\beta(T_{i1}\phi_\xi + T_{i2}\phi_\eta + T_{i3}\phi_\zeta)|_\sigma^{\mathrm{R}} \tag{12}$$

for each interface. Here $\beta = 1/n_f$ where n_f is the number of subcell faces making one interior surface that slices through a primal cell, e.g. for a hexahedra $n_f = 4$. The general tensor $\mathbf{T}$ of Equation (6) is approximated locally by resolving full-tensor fluxes with respect to the subcell geometry and control-volume permeability. The flux continuity equations Equation (12) define a local system of equations for the interface pressures, where the number of continuity equations matches the number of interface pressures and is equal to the number of edges of the primal cell. The discrete pressure field has a piecewise linear variation over each subcell tetrahedra and consequently approximations of the derivatives ϕ_ξ, ϕ_η and ϕ_ζ are linear functions of $\mathbf{\Phi}_f$ and $\mathbf{\Phi}_v$. Here $\Gamma|_\sigma^j$ denotes interface flux Γ at location σ and state of volume j. The actual position of σ on each subcell face defines both the point of continuous pressure and the flux quadrature, and in turn leads to a family of schemes analogous to Reference [18].

The development of these schemes raises many interesting issues, which are being investigated in current research. In this paper flux continuity conditions are restricted to tetrahedral and hexahedral cells and the base members of the families of schemes with quadrature $q = 1$ (defined in References [12, 18]) are tested. Pyramids (which require special treatment) and prisms are currently only used in regions where permeability tensors are constant, as in the test cases presented in the results section. The current pyramid and prism fluxes are built using the correct local cell geometry and remain consistent and locally conservative with respect to control-volumes provided the permeability tensor is constant throughout these cells. The development of full flux continuity conditions that allow the permeability tensor to vary inside these cells, i.e. to jump across control-volume faces inside pyramid and prism cells is beyond the scope of this paper and will be presented in a future report.

DOI: 10.1002/fld

The algebraic system of fluxes of Equation (12) are rearranged in the form

$$\mathbf{F} = A_{\mathrm{L}}\mathbf{\Phi}_f + B_{\mathrm{L}}\mathbf{\Phi}_v = A_{\mathrm{R}}\mathbf{\Phi}_f + B_{\mathrm{R}}\mathbf{\Phi}_v \tag{13}$$

and thus the interface pressures can be expressed *locally* in terms of the cell vertex pressures. After elimination of the Φ_f from Equation (13) it follows that

$$\mathbf{F} = (A_{\mathrm{L}}(A_{\mathrm{L}} - A_{\mathrm{R}})^{-1}(B_{\mathrm{R}} - B_{\mathrm{L}}) + B_{\mathrm{L}})\mathbf{\Phi}_v \tag{14}$$

The fluxes of Equation (14) can be written as a linear combination of cell edge potential differences [12] and satisfy the consistency condition that the flux is zero for constant potential.

4. HIGHER-ORDER MULTI-PHASE FLOW APPROXIMATIONS

The general finite volume discretization of Equation (1) for multi-phase flow on unstructured grids takes the form

$$(S_{p_i}^{n+1} - S_{p_i}^{n})\tau_i + \Delta t \sum_{j=1}^{N_{\mathrm{edV}}} \mathrm{f}_p(\mathbf{S}_{\mathrm{L}}^{n+q}, \mathbf{S}_{\mathrm{R}}^{n+q}) F_{T_{e(i,j)}}(\phi^{n+1}) = \Delta t M_{p_i} \tag{15}$$

for the pth phase continuity equation, where $\mathbf{S}_{\mathrm{L}}^{n+q}, \mathbf{S}_{\mathrm{R}}^{n+q}$ are the left- and right-hand phase saturation vectors with respect to edge $e(i, j)$ and $n + q$ denotes the time level of the scheme. Here $F_{T_{e(i,j)}} = \Lambda F_{e(i,j)}(\phi)$ and M_{p_i} denotes the pth phase flow rate, prescribed at wells and is zero otherwise. The phase continuity equations are coupled through the discrete pressure equation

$$\sum_{j=1}^{N_{\mathrm{edV}}} \Lambda(\mathbf{S}_{\mathrm{L}}^{n+q}, \mathbf{S}_{\mathrm{R}}^{n+q}) F_{e(i,j)}(\phi^{n+1}) = M_i \tag{16}$$

The system Equations (15), (16) are solved implicitly with $q = 1$ in this work. Implicit flux limiting schemes for reservoir simulation have been presented in Reference [15], where a weighted Crank-Nicolson scheme is developed [5] for time accuracy. The sequential scheme with $q = 0$ corresponding to implicit pressure explicit saturation (IMPES), which is far more common for higher order schemes can also be used. Time accuracy of the methods are under development. A common approach is the use of the Runge–Kutta method [33] for the explicit time integration of the convective equations.

The approximate flux is defined according to the sign of the local wave direction w_p, evaluated here at the edge mid-point. Referring to Figure 3,with respect to a local frame of reference aligned with the direction i to k along the edge vector $\Delta\mathbf{r}_{k,i}$, the standard reservoir simulation upwind scheme is written as

$$\mathrm{f}_p(\mathbf{S}_{\mathrm{L}}^{n+q}, \mathbf{S}_{\mathrm{R}}^{n+q}) = \begin{cases} \mathrm{f}_p(\mathbf{S}_{\mathrm{L}}^{n+q}), & w_p \geqslant 0 \\ \mathrm{f}_p(\mathbf{S}_{\mathrm{R}}^{n+q}), & w_p < 0 \end{cases} \tag{17}$$

and the first-order upwind scheme, (known as single-point upstream weighting in the reservoir simulation literature [1]) is defined with $\mathbf{S}_{\mathrm{L}}^{n+q} = \mathbf{S}_i^{n+q}$ and $\mathbf{S}_{\mathrm{R}}^{n+q} = \mathbf{S}_k^{n+q}$.

DOI: 10.1002/fld

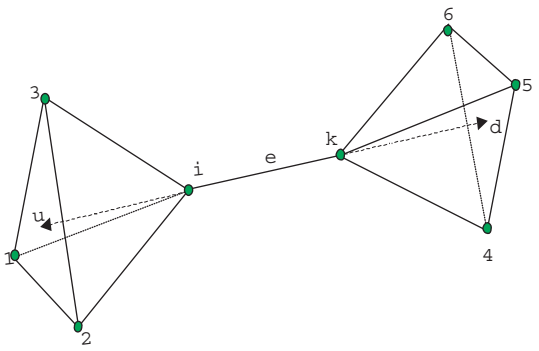

Figure 3. Higher order support.

4.1. Higher order schemes

A three-dimensional higher order approximation is now introduced with respect to the saturation variables. From here on it is understood that all saturations are computed at level $n+q$ depending on the choice of scheme formulation. The scheme is expressed in two-steps. Higher order left- and right-hand side states are defined relative to the mid-point of each edge e (along which flux is to be defined) by expansions about the edge vertices at i and k, Figure 3. As in Reference [3], the expansions are constrained with slope limiters to ensure that the higher order data satisfies a local maximum principle, preventing the introduction of spurious extrema.

First we define the difference in $\mathbf{S}$ over the edge e Figure 3, as

$$\Delta\mathbf{S}_{ki} = \mathbf{S}_k - \mathbf{S}_i \tag{18}$$

where it is now understood that $\Delta\mathbf{S}$ with a double suffix denotes a difference in $\mathbf{S}$. Referring to Figure 3 the left and right states $\mathbf{S}_{\mathrm{L}}$ and $\mathbf{S}_{\mathrm{R}}$ at the mid-point of the *key* edge e (joining vertices i and k) are expressed as

$$\mathbf{S}_{\mathrm{L}} = \mathbf{S}_i + \tfrac{1}{2}\Phi^{+}\Delta\mathbf{S}_{ki} \tag{19}$$

where Φ^{+} is a function of

$$\mathbf{r}_{ki}^{+} = (\Delta\mathbf{S}_{iu}/\Delta\mathbf{S}_{ki}) \tag{20}$$

and

$$\mathbf{S}_{\mathrm{R}} = \mathbf{S}_k - \tfrac{1}{2}\Phi^{-}\Delta\mathbf{S}_{ki} \tag{21}$$

where Φ^{-} is a function of

$$\mathbf{r}_{ki}^{-} = (\Delta\mathbf{S}_{dk}/\Delta\mathbf{S}_{ki}) \tag{22}$$

The differences $\Delta\mathbf{S}_{iu}$ and $\Delta\mathbf{S}_{dk}$ are well defined on a structured grid.

However extension to unstructured grids requires special construction of the differences $\Delta\mathbf{S}_{iu}$ and $\Delta\mathbf{S}_{dk}$.

DOI: 10.1002/fld

Directional differences are constructed by extrapolating along the *key* edge defined by vector $\Delta\mathbf{r}_{ki}$ in the respective upstream and downstream directions, see arrows in Figure 3. The procedure is illustrated for tetrahedral cells.

Extrapolation of the respective upstream and downstream data is constrained such that a local maximum principle holds for a scalar equation. The upstream tetrahedra i, 1, 2, 3 is labelled T_{U} and the down stream tetrahedra k, 4, 5, 6 is labelled T_{D}. The space vector corresponding to edge e ($d\mathbf{r}_{ki}$) is extrapolated into the respective tetrahedra T_{U}, T_{D}, see arrows in Figure 3. This is illustrated further with respect to vertex i. The edge vector is extrapolated to the point of intersection u, on the opposite face of the tetrahedra T_{U}, Figure 3. The *upwind* difference is then obtained via the expansion

$$\Delta\mathbf{S}_{iu} = \nabla\mathbf{S}_{T_{\mathrm{U}}} \cdot \mathrm{d}\mathbf{r}_{iu} \tag{23}$$

and for a linear approximation of $\mathbf{S}$ over the tetrahedra T_{U} the right-hand side of Equation (23) is equal to the convex average of tetrahedral edge differences with

$$\Delta\mathbf{S}_{iu} = \xi_1\Delta\mathbf{S}_{i1} + \xi_2\Delta\mathbf{S}_{i2} + \xi_3\Delta\mathbf{S}_{i3} \tag{24}$$

where ξ_i, $i = 1, \ldots, 3$ are the ratio of volumes of sub-tetrahedra defined in T_{U} with respective base areas $(u, 3, 2)$, $(u, 1, 3)$, $(u, 2, 1)$, to volume of tetrahedra T_{U} and are therefore positive and sum to unity. In order to impose a maximum principle with respect to T_{U} and edge e, the limiter Φ^+ is defined by

$$\Phi^+ = \phi(r_{ki}^+) \tag{25}$$

where r_{ki}^+ is defined by Equation (32) and $\phi(r)$ is any classical slope limiter [36, 37]. The higher order reconstruction is then bounded between $\mathbf{S}_k$ and $\mathbf{S}_u$. By convexity (Equation (24)) $\mathbf{S}_u = \xi_1\mathbf{S}_1 + \xi_2\mathbf{S}_2 + \xi_3\mathbf{S}_3$, thus bounds are such that

$$\min_{T_{\mathrm{U}}\cup e}\mathbf{S} \leqslant \mathbf{S}_{\mathrm{L}} \leqslant \max_{T_{\mathrm{U}}\cup e}\mathbf{S} \tag{26}$$

over tetrahedra T_{U} and edge e yielding a local maximum principle with reconstruction reducing to first order locally at three dimensional extrema. In cases where coincidence or near coincidence is detected between the extrapolated edge and an upwind tetrahedral face or edge the limiting is collapsed to be entirely face or edge based. A similar convex average interpolant is constructed with respect to vertex k using the right hand tetrahedra T_{D} to obtain the difference $\Delta\mathbf{S}_{dk}$ together with analogous limiter bounds that now depend on the edge slopes $\Delta\mathbf{S}_{4k}$, $\Delta\mathbf{S}_{5k}$ and $\Delta\mathbf{S}_{6k}$ ensuring a maximum principle with $\min\mathbf{S} \leqslant \mathbf{S}_{\mathrm{R}} \leqslant \max\mathbf{S}$ over T_{D} and edge e.

This scheme is a three-dimensional generalization of the higher order scheme presented in Reference [3] and is similar in motivation to the local edge diminishing (LED) schemes of References [34, 35], with a higher order reconstruction applied to the data, (saturation field in this case). The second step of the scheme uses the upwind flux where each higher order approximation of phase saturation is upwinded via the flux using Equations (19), (21) in Equation (17). The van-Leer (Fromm) limiter [36]

$$\phi(r) = \max\left(0, \min\left(2r, 2, \frac{(1+r)}{2}\right)\right) \tag{27}$$

DOI: 10.1002/fld

is used to define $\phi(r)$ in Equation (25), other possible limiters are presented in Reference [37, 38]. Note as before, that the first-order flux is recovered locally if the limiters are set to zero.

5. RESULTS

The test cases involve two phase flow (oil–water) initial oil saturation is prescribed and water is injected. Water saturation contours are shown in each case. Solid wall (zero normal flow) boundary conditions are applied on all exterior boundaries of each reservoir domain. The grids employed here are fairly smooth although major changes in grid type occur. In all cases flow rate is specified at the (inflow) injector and pressure is prescribed at the (outflow) producer.

5.1. Case 1

This case involves a three-dimensional grid orientation study, using a prismatic grid Figure 4. The tensor is assumed to be diagonal isotropic. Injection and production wells are located half way along diagonally opposite edges of the hexahedral domain, Figure 4. Water saturation contours are shown at 0.95 PV injected, view from the injector in Figure 5 and view from producer in Figure 6. The result obtained with a consistent Darcy flux approximation and first-order convective flux is shown in Figures 5(a) and 6(a), respectively. The contours indicate a non-symmetric profile, both

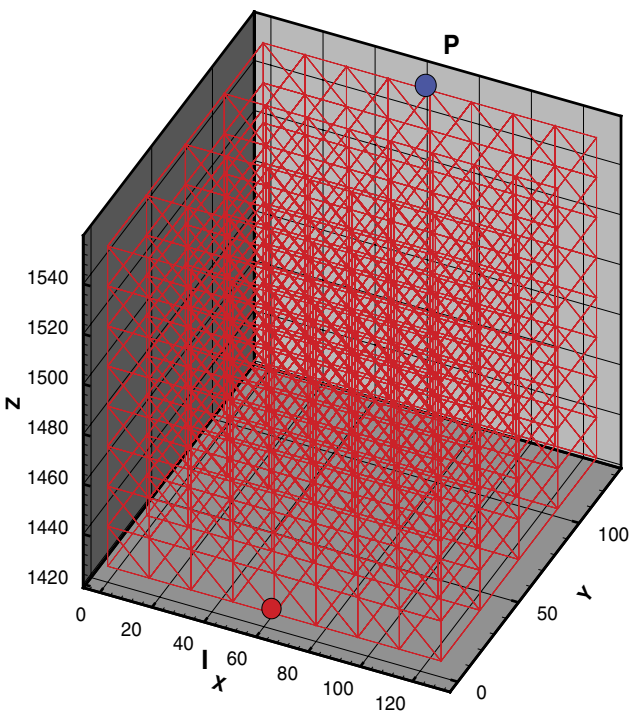

Figure 4. Prismatic grid and boundary conditions.

DOI: 10.1002/fld

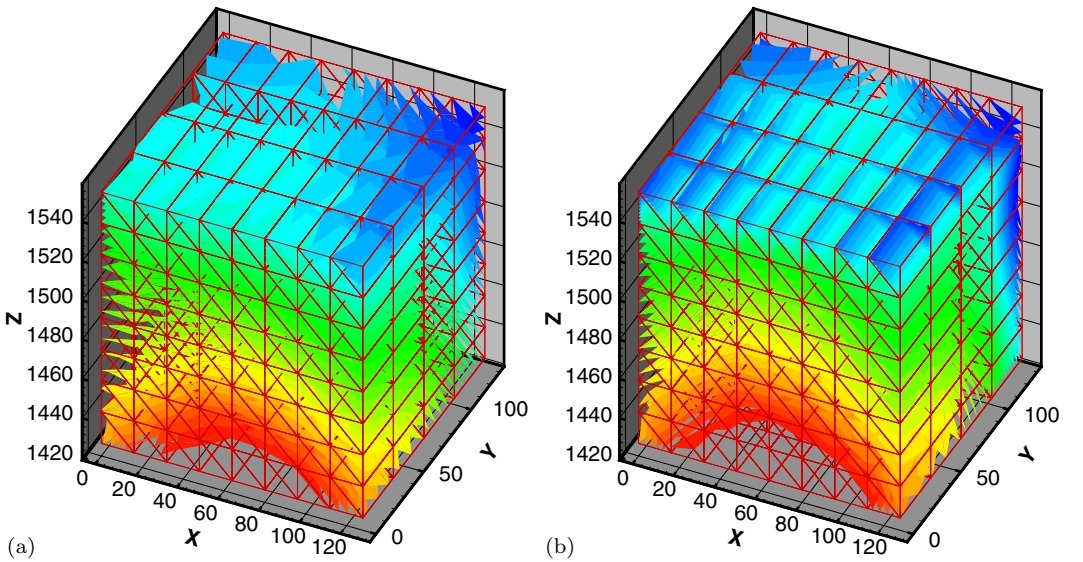

Figure 5. 3D water saturation contours—prism grid orientation test: (a) CVD first order; and (b) CVD higher order.

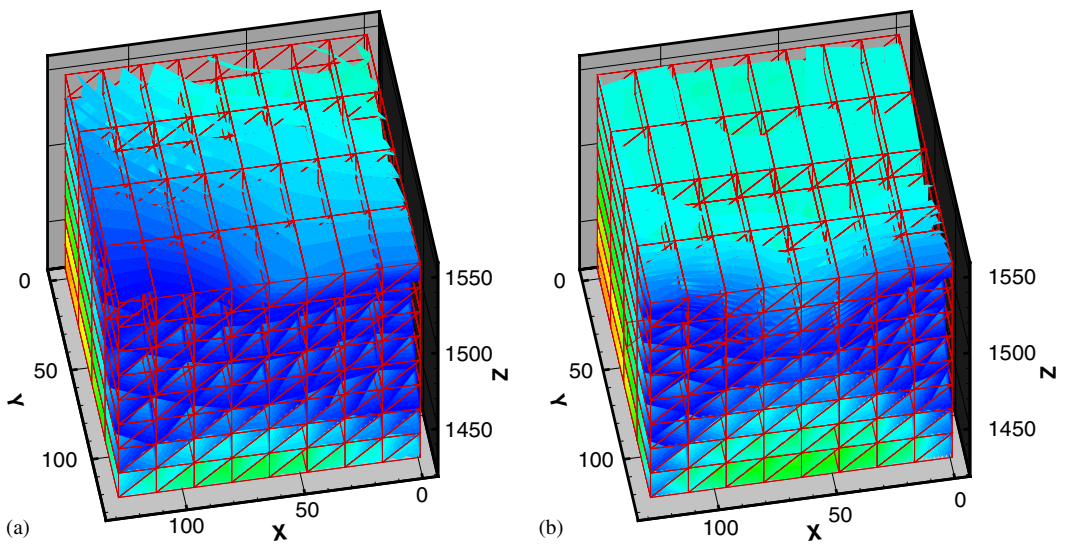

Figure 6. 3D water saturation contours—prism grid orientation test: (a) CVD first order; and (b) CVD higher order.

on the domain face adjacent to the edge on which the injector is placed and on the upper surface where contours are seen to be non-symmetric about the centre line towards the producer. This result shows a fully three-dimensional grid orientation effect is induced by the prismatic cells when

DOI: 10.1002/fld

using a first-order upwind scheme. The result obtained with a consistent Darcy flux approximation and higher order convective flux is shown in Figures 5(b), and 6(b), respectively. The higher order scheme provides considerable improvement in resolution of the Buckley Leverett shock front and yields an almost symmetric profile demonstrating the need for both a consistent Darcy flux approximation and higher order convective flux on unstructured grids in three dimensions.

5.2. *Case 2*

The following example illustrates a fundamental difference in behaviour between the above CVD formulation and CVFE [32]. In contrast to the CVD schemes where flow variables and rock properties are assigned to the control-volumes, the CVFE formulation assigns flow variables to the vertices and rock properties to the cells or elements. The CVFE formulation is not flux continuous in general and it is well known that this type of approximation can cause spreading of information when rapid changes in rock properties occur e.g. References [3, 39, 40]. This example shows that while higher order fluid transport approximations can improve a low-order result, the higher order schemes do not compensate for the loss of information inherent in the CVFE Darcy flux.

The test case involves three-dimensional flow in a domain comprised of a mixed hybrid grid of hexahedral cells and tetrahedral cells joined by an interface comprised of a layer of pyramid cells. The domain and boundary conditions (injector lower right-hand corner and producer upper left-hand corner) are indicated in Figures 7 (CVFE grid) and 8 (CVD grid). The domain is assigned a high permeability field and is divided by a low permeability layer with drop by six orders of magnitude in permeability. The layer is in the $(y–z)$ plane at $x = 95$, with an aperture (position

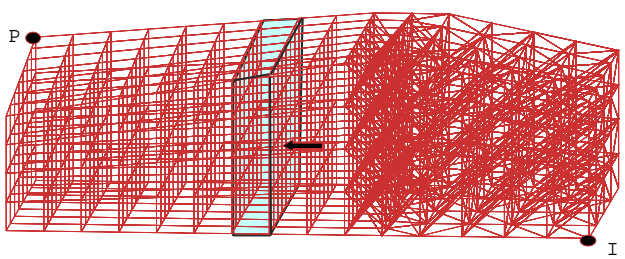

Figure 7. Hybrid Hex-Tet and pyramid layer grid with low-perm barrier and aperture CVFE grid.

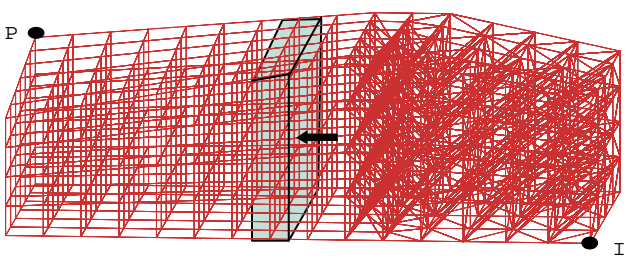

Figure 8. Hybrid Hex-Tet and pyramid layer grid with low-perm barrier and aperture CVD grid.

DOI: 10.1002/fld

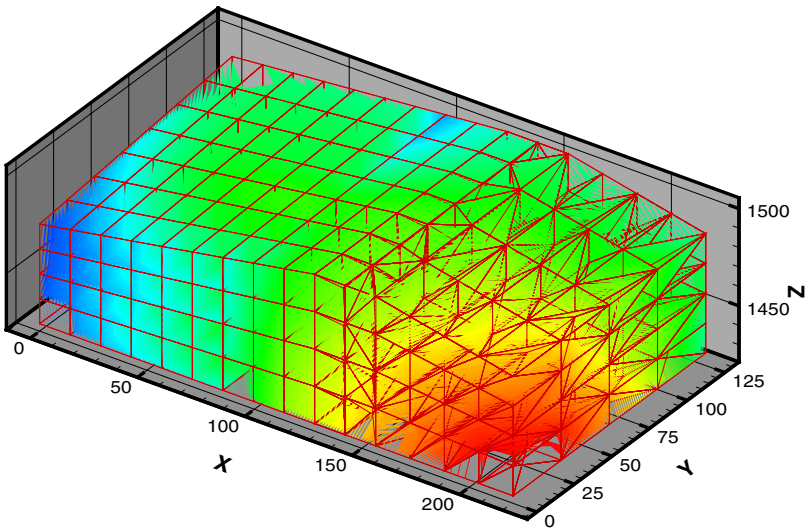

Figure 9. 3D water saturation contours—hybrid Hex-Tet and pyramid layer CVFE first order.

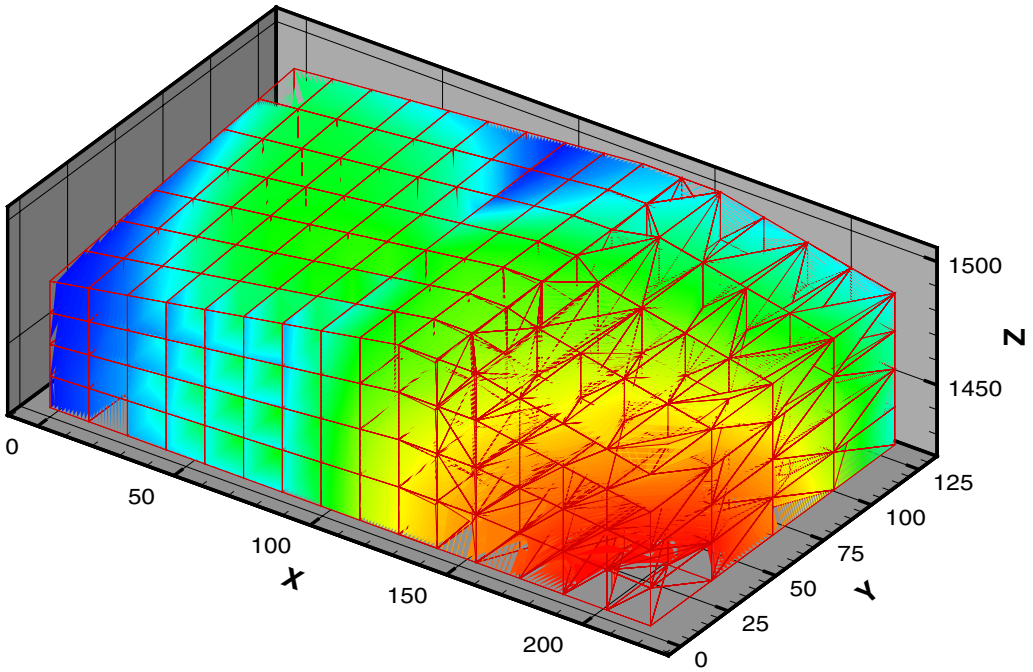

Figure 10. 3D water saturation contours—hybrid Hex-Tet and pyramid layer CVFE higher order.

indicated by arrows) approximately in the centre of the layer of one control-volume in size, Figures 7 and 8.

The low and higher order CVD schemes are compared with the low and higher order CVFE schemes for this case at 0.75 PV injected. The CVFE and CVD grids are shown in Figures 7 and 8.

DOI: 10.1002/fld

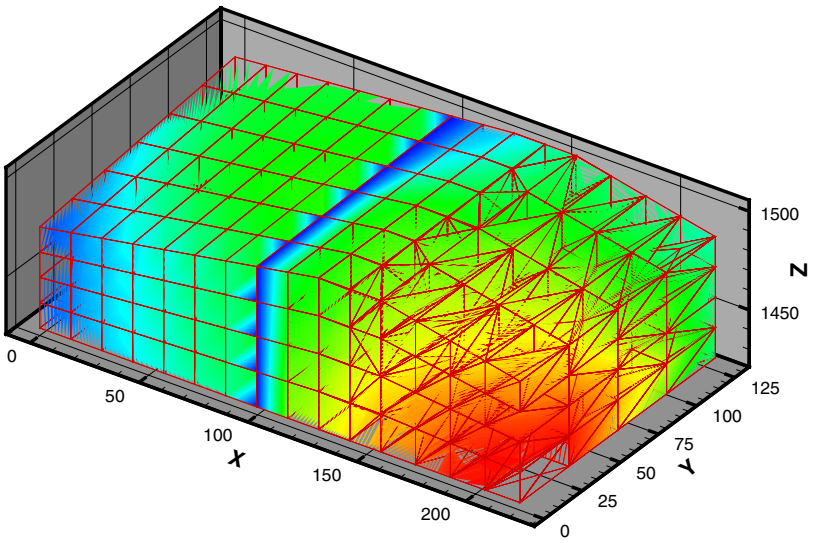

Figure 11. 3D water saturation contours—hybrid Hex-Tet and pyramid layer CVD first order.

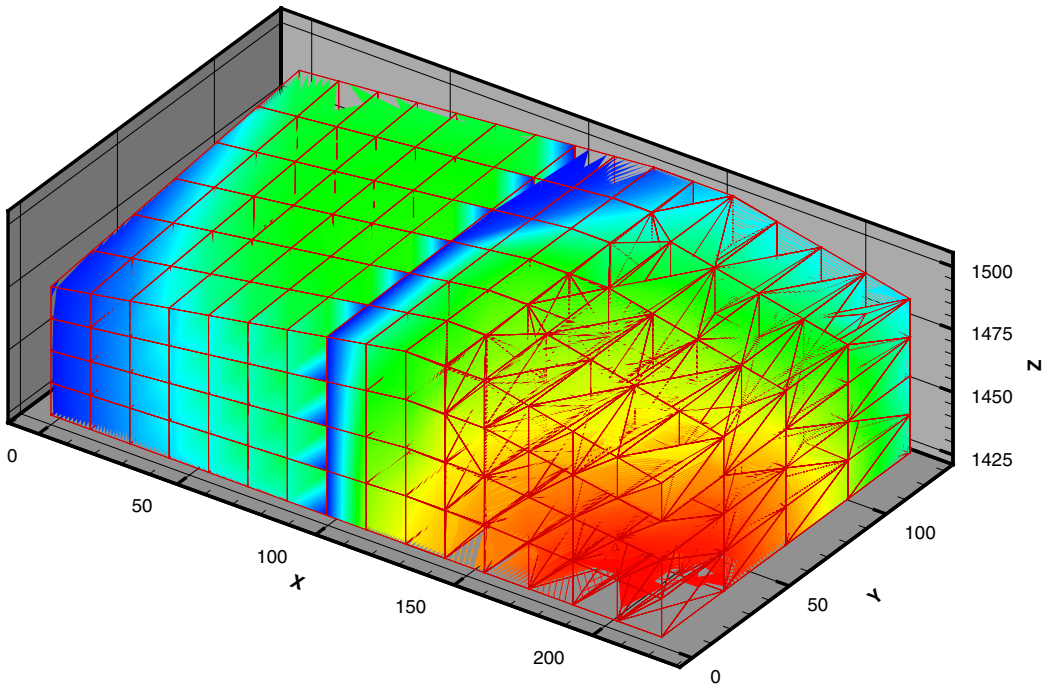

Figure 12. 3D water saturation contours—hybrid Hex-Tet and pyramid layer CVD higher order.

DOI: 10.1002/fld

As in two dimensions [3], the grids are chosen so as to approximately maintain the same problem and permeability variation with respect to the scheme formulations. Permeability is assigned to the control-volumes of the CVD grid. The CVFE grid is given an extra layer of cells across the domain so that the aperture is comparable with that of the CVD grid and permeability is defined cell-wise over the CVFE grid.

First order and higher order CVFE results are shown in Figures 9 and 10, respectively. The respective CVD results are shown in Figures 11 and 12. The first-order CVFE scheme result shows strong flow through the low permeability barrier, which should remain essentially no-flow in the region away from the aperture, Figure 9. In sharp contrast, the resolution of the flow in the neighbourhood of the low permeability barrier is evident in the case of the first order CVD scheme Figure 11, with the flux continuous CVD scheme providing much clearer resolution of flow and trapped oil near the low permeability barrier.

While the higher order CVFE scheme Figure 10 yields a sharper shock front than the first-order CVFE scheme Figure 9, the higher order scheme cannot compensate for the basically incorrect trend in flow behaviour predicted by the CVFE scheme. The averaging effect that is inherent in the CVFE Darcy flux approximation still induces significant flow through the low permeability barrier despite the use of a higher order convective flux. Consequently, while the shock front is sharper the flow field is quite different to that of the CVD scheme.

The higher order CVD scheme Figure 12 provides further improvement in resolution of the flow field compared to the first-order CVD scheme Figure 11. The low permeability barrier is clearly detected by the higher order CVD scheme and resolution of the front is also improved throughout the unstructured grid domain. The difference between higher order CVD (Figure 12) and higher order CVFE (Figure 10) serves to again highlight the benefits of the CVD formulation which uses the same number of degrees of freedom for flow variable approximation.

6. CONCLUSIONS

A novel higher order convective flux approximation is presented for unstructured grids in three dimensions. The resulting higher order convective flux approximations are coupled with consistent and efficient continuous Darcy flux approximations. The coupling leads to new schemes for reservoir simulation on quite general structured and unstructured grids that can be comprised of tetrahedra, pyramids, prisms and hexahedra.

Benefits of the new higher order CVD schemes are demonstrated by comparisons with current methods in reservoir simulation and with the standard control-volume finite element CVFE scheme which uses the same number of degrees of freedom as the new schemes.

Results are presented for two phase flow in three dimensions which clearly show that the higher order schemes improve front resolution and significantly reduce unstructured grid orientation effects.

The CVFE scheme tends to average flow effects in the presence of rapid changes in permeability on grids of finite level. While the higher order CVFE scheme improves front resolution compared to first order CVFE, the higher order CVFE scheme cannot compensate for loss of crucial Darcy flux information that occurs as a consequence of the CVFE formulation, consistent with earlier findings in 2-D.

DOI: 10.1002/fld

In addition to improved front resolution the higher order CVD scheme is shown to significantly improve flow resolution in the presence of medium discontinuities in three-dimensional problems.

ACKNOWLEDGEMENTS

The referees are thanked for their helpful comments. Support of EPSRC grant GR/S70968/01 is gratefully acknowledged.

REFERENCES

1. Aziz K, Settari A. *Petroleum Reservoir Simulation*. Applied Science Publishers: London, 1979.
2. Bear J. *Dynamics of Fluids in Porous Media*. American Elsevier: New York, 1972.
3. Edwards MG. Higher-resolution hyperbolic-coupled-elliptic flux-continuous CVD schemes on structured and unstructured grids in 2-D. *International Journal for Numerical Methods in Fluids*, submitted.
4. Bell JB, Colella P, Trangenstein JA. Higher order Godunov methods for general systems of hyperbolic conservation laws. *Journal of Computational Physics* 1989; **82**:362–397.
5. Blunt MJ, Rubin B. Implicit flux-limiting schemes for petroleum reservoir simulation. *Journal of Computational Physics* 1992; **102**:194–210.
6. Edwards MG, Christie MA. Dynamically adaptive Godunov schemes with renormalization for reservoir simulation. *Proceedings of the Twelfth SPE Reservoir Simulation Symposium*, *SPE 25268*, New Orleans, Louisiana, U.S.A., 28 February–3 March 1993; 413–422.
7. Durlofsky LJ. A triangle based mixed finite element finite volume technique for modeling two phase flow through porous media. *Journal of Computational Physics* 1993; 252–266.
8. Edwards MG. A higher order Godunov scheme coupled with dynamic local grid refinement for flow in a porous medium. *Computer Methods in Applied Mechanics and Engineering* 1996; **131**:287–308.
9. Edwards MG. Cross-flow, tensors and finite volume approximation with deferred correction. *Computer Methods in Applied Mechanics and Engineering* 1998; **151**:143–161.
10. Thiele M, Edwards MG. Physically based higher order Godunov schemes for compositional simulation. *Proceedings of the SPE Reservoir Simulation Symposium*, *Paper 66403*, Houston, TX, U.S.A., 11–14 February 2001.
11. Edwards MG. Non-upwind versus upwind schemes for hyperbolic conservation laws in porous media. *Proceedings of the SPE Reservoir Simulation Symposium*, *Paper 93691*, Houston, TX, U.S.A., 31 January–2 February 2005.
12. Edwards MG. Unstructured, control-volume distributed, full-tensor finite volume schemes with flow based grids. *Computational Geosciences* 2002; **6**:433–452.
13. Edwards MG. Symmetric positive definite general tensor discretization operators on unstructured and flow based grids. *Proceedings of the ECMOR VIII*, *8th European Conference on the Mathematics of Oil Recovery*, Frieberg, Germany, 3–6 September 2002.
14. Edwards MG. Control-volume distributed sub-cell flux schemes for unstructured and flow based grids. *SPE Reservoir Simulation Symposium*, Houston, Texas, U.S.A., 3–5 February 2003.
15. Edwards MG. Split full tensor discretization operators for structured and unstructured grids in three dimensions. *Proceedings of the SPE Reservoir Simulation Symposium Houston*, *SPE 66358*, Texas, 11–14 February 2001.
16. Edwards MG. M-matrix flux splitting for general full tensor discretization operators on structured and unstructured grids. *Journal of Computational Physics* 2000; **160**:1–28.
17. Edwards MG. Simulation with a full-tensor coefficient velocity field recovered from a diagonal tensor solution. *SPE Journal* 2000; **5**:387–393.
18. Edwards MG, Rogers CF. Finite volume discretization with imposed flux continuity for the general tensor pressure equation. *Computational Geosciences* 1998; **2**:259–290.
19. Aavatsmark I. Introduction to multipoint flux approximation for quadrilateral grids. *Computational Geosciences* 2002; **6**:405–432.
20. Aavatsmark I, Barkve T, Mannseth T. Control-volume discretization methods for 3D quadrilateral grids in inhomogeneous, anisotropic reservoirs. *SPE Reservoir Simulation Symposium*, Dallas, TX, U.S.A., 1997.
21. Aavatsmark I, Barkve T, Bøe Ø, Mannseth T. Discretization on unstructured grids for inhomogeneous, anisotropic media. Part 1. Methods. *SIAM Journal on Scientific Computing* 1998; **19**:1700–1716.

DOI: 10.1002/fld

22. Aavatsmark I, Barkve T, Bøe Ø, Mannseth T. Discretization on unstructured grids for inhomogeneous, anisotropic media. Part II. Results. *SIAM Journal on Scientific Computing* 1998; **19**:1717–1736.
23. Verma S, Aziz K. A control volume scheme for flexible grids in reservoir simulation. *14th SPE Reservoir Simulation Symposium*, *SPE 37999*, Dallas, Texas, U.S.A., 8–11 June 1997; 215, 227.
24. Lee SH, Durlofsky LJ, Lough MF, Chen W. Finite difference simulation of geologically complex reservoirs with tensor permeabilities. *SPE Reservoir Simulation Symposium*, *SPE 38002 1997*, Dallas, TX, U.S.A.
25. Lee SH, Tchelepi H, DeChant LJ. Implementation of a flux continuous finite difference method for stratigraphic hexahedron grids. *Proceedings of the SPE Reservoir Simulation Symposium*, *Paper SPE 51901*, Houston, Texas, U.S.A., 14–17 February 1999.
26. Pal M, Edwards MG, Lamb AR. Convergence study of a family of flux-continuous, finite schemes for the general tensor pressure equation. *International Journal for Numerical Methods in Fluids*, submitted.
27. Arbogast T, Wheeler MF, Yotov I. Mixed finite elements for elliptic problems with tensor coefficients as cell centered finite differences. *SIAM Journal on Numerical Analysis* 1997; **34**(2):828.
28. Raviart RA, Thomas JM. *A Mixed Finite Element Method for Second-Order Problems*. Lecture Notes in Mathematics, vol. 606. Springer: New York, 1977; 292–315.
29. Russel TF, Wheeler MF. Finite element and finite difference methods for continuous flows in porous media. In *Mathematics of Reservoir Simulation* (Chapter 2), Ewing RD (ed.), Frontiers in Applied Mathematics. SIAM: Philadelphia, PA, 1983; 35–106.
30. Farmer CL, Heath DE, Moody RO. A global optimization approach to grid generation. *11th SPE Reservoir Simulation Symposium*, Anaheim, CA, U.S.A., 17–20 February 1991; 341–350.
31. Russell TF. Relationships among some conservative discretization methods. In *Numerical Treatment of Multiphase Flows in Porous Media*, Chen Z *et al*. (eds). Lecture Notes in Physics, vol. 552. Springer: Heidelberg, 2000; 267–282.
32. Forsyth P. A control-volume finite element method for local mesh refinement in thermal reservoir simulation. *SPERE*, November 1990; 561.
33. Shu CW, Osher S. Efficient implementation of essentially non-oscillatory shock capturing schemes. *Journal of Computational Physics* 1988: **77**:439–471.
34. Jameson A. Artificial diffusion, upwind biasing, limiters and their effect on accuracy and multigrid convergence in transonic and hypersonic flows. *AIAA 93-3359*, 1993.
35. Lyra P, Morgan K. A review and comparative study of upwind biased schemes for compressible flow computation. Part III: Multidimensional extension on unstructured grids. *Archives of Computational Methods in Engineering*, 2002; **9**(3):207–256.
36. van Leer B. Towards the ultimate conservative difference scheme V. A sequel to Godunov's method. *Journal of Computational Physics* 1979; **32**:101–136.
37. Sweby P. High resolution schemes using flux limiters for hyperbolic conservation laws. *SIAM Journal on Numerical Analysis* 1984; **21**:995–1011.
38. Godlewski E, Raviart P. *Numerical Approximation of Hyperbolic Systems of Conservation Laws*. Applied Mathematical Science, vol. 118. Springer: New York, 1996.
39. Prevost M, Edwards MG, Blunt MJ. Streamline tracing on curvilinear structured and unstructured grids. *SPE Journal* 2002.
40. Klausen R, Eigstad G. Multipoint flux approximations and finite element methods; practical aspects of discontinuous media. *ECMOR VIII Proceedings*: *9th European Conference on the Mathematics of Oil Recovery*, Cannes, France, 30 August–2 September 2004.

DOI: 10.1002/fld